Received: 28 February 2022 | Revised: 16 August 2022 | Accepted: 5 September 2022

DOI: 10.1111/andr.13292

ANDROLOGY WILEY

ORIGINAL ARTICLE

The murine male reproductive organ at a glance: Three-dimensional insights and virtual histology using label-free light sheet microcopy

Diana Pinkert-Leetsch[1,2] | John Uwe Rost[1] | Max Ulrich Heiner Schmiedeknecht[3] | Christine Stadelmann[3,5] | Frauke Alves[1,2,4,5] | Jeannine Missbach-Guentner[1]

[1]Department of Diagnostic and Interventional Radiology, University Medical Center Goettingen, Goettingen, Germany

[2]Translational Molecular Imaging, Max-Planck-Institute for Multidisciplinary Sciences, Goettingen, Germany

[3]Department of Neuropathology, University Medical Center Goettingen, Goettingen, Germany

[4]Department of Hematology and Medical Oncology, University Medical Center Goettingen, Goettingen, Germany

[5]Cluster of Excellence "Multiscale Bioimaging: from Molecular Machines to Networks of Excitable Cells" (MBExC), University of Goettingen, Robert-Koch-Str. 40, Goettingen, Germany

Correspondence
Jeannine Missbach-Guentner, Department of Diagnostic and Interventional Radiology, University Medical Center Goettingen, Goettingen, Germany.
Email: j.missbach@med.uni-goettingen.de

Funding information
Bundesministerium fuer Bildung und Forschung, Deutschland, Grant/Award Numbers: 13N14349, 13N143450; Deutsche Forschungsgemeinschaft, Grant/Award Number: EXC 2067/1-390729940

Abstract

Background: The unique anatomy of the male reproductive organ reflects its complex function from sperm maturation to their storage for months until emission. Since light microscopy in two dimensions (2d) cannot sufficiently demonstrate its complex morphology, a comprehensive visualization is required to identify pathologic alterations in its entire anatomical context.

Objectives: Aim of this study was to use three-dimensional (3d) light sheet fluorescence microscopy (LSFM) to visualize entire murine testes in 3d, label-free and at subcellular resolution, and to assign local autofluorescence to testicular and deferent structures.

Materials and methods: Murine testes were fixed with four different fixatives and subsequently cleared with benzoic acid/benzyl benzoate. Hereafter, complete murine testes were scanned with LSFM with different fluorescence filter sets and subsequently embedded in paraffin for further conventional planar histology.

Results: Autofluorescence signals of the murine reproductive organ allowed the unambiguous identification of the testicular anatomy from the seminiferous tubules to the vas deferens with their specific stratification independent of the used fixative. Blood vessels were visualized from the pampiniform plexus to the small capillaries of single tubules. Moreover, due to the specific intrinsic fluorescence properties of the efferent ducts and the epididymis, luminal caliber, the epithelial stratification and retronuclear cytoplasmic inclusions gave a unique insight into the interface of both morphological structures. Subsequent 2d histology confirmed the identified morphological structures.

Discussion: LSFM analysis of the murine reproductive organ allows due to its intrinsic fluorescence a simple, label-free 3d assessment of its entire duct morphology, the epithelial composition, and the associated blood supply in its anatomical relation.

Conclusion: LSFM provides the technical basis for comprehensive analyses of pathologically altered murine testes in its entirety by depicting specific autofluorescence. Thereby it facilitates mouse studies of testicular disease or their drug-related alterations in more detail potentially for clinical translation assessing human testicular biopsies.

KEYWORDS
3d virtual histology, autofluorescence, light sheet fluorescence microscopy, male reproductive organ, testis

1 | INTRODUCTION

The unique anatomy of the male reproductive organ is an expression of its multifaceted function, which is reflected in a complex morphology. The testis is the site of sperm production, but at the same time, it is also the site of sperm differentiation and maturation.

The convoluted, highly extensive channel system of the testis and the associated ducts allow the maturation and storage of sperm for months until emission. However, this delicate and complex organ is prone to morphological alterations and neoplasia, due to environmental impacts, endocrine imbalances and physical trauma.[1–3] This organ complexity with all its manifold pathologies also requires particularly extensive and meaningful diagnostics.

The first choice in clinical imaging for evaluation of the testis is Color Doppler ultrasonography (CDUS).[4] In case of an equivocal CDUS finding, multiparametric magnetic resonance imaging (mpMRI) follows as a second imaging modality, which can differentiate between intra-testicular and para-testicular lesions due to its excellent resolution.[5] Both imaging modalities do not use ionizing radiation and are therefore particularly suitable for imaging the radiosensitive testis. However, neither CDUS nor mpMRI provide cellular resolution and therefore cannot replace biopsies for the evaluation of various scrotal pathologies. In addition, in Western societies, there is an increasing need for comprehensive diagnostics to clarify infertility in particular[6] but also for specific diagnosis of biopsies from scrotal neoplasms.

Two-dimensional (2d) light microscopic examinations of the structure of the testis do not sufficiently represent the complex structure of the testis. Therefore, a three-dimensional (3d) examination would be desirable for comprehensive analysis of the entire biopsy volume to visualize morphological alterations, resulting in infertility, caused by neoplasms or trauma within the anatomical relationships of testicular structures.

To gain these necessary 3d insights into the tissue structure, reconstructions of the adjacent ductal systems of the efferent ducts and epididymis were made based on many sequential 2d histological sections and summed as a 3d data set.[7] In an alternative technical approach, the tubules of the epididymis were segmented from paraffin sections and traced along their entire length to obtain a spatial impression of the entire epididymis.[8] Despite the gained 3d representation, both studies required an immense technical and computational effort. Innovative imaging diagnostics emerge in the field of preclinical research and use animal models to enable clinical translation at a later stage.

Here, preclinical experimental imaging techniques such as micro-computed tomography (μCT) or synchrotron radiation-based CT offer a true 3d virtual histology and in combination with phase contrast, a resolution down to cell level. These μCT approaches allow the imaging of entire murine organs or tumors and human biopsies of mammary and pancreatic tumors.[9,10] Depending on the used X-ray source, a contrast enhancement using, for example, phosphotungstic acid is necessary in order to depict specific density distributions within the soft tissue, for example, the qualitative and quantitative analysis of murine fibrotic kidneys[11] and atherosclerotic plaques in mouse hearts.[12] However, a disadvantage of X-ray-based virtual histology is the complex technical apparatus and the necessary application of ionizing radiation. In contrast, fluorescence-based light sheet microscopy (LSFM) is a further imaging strategy that provides a comprehensive 3d tissue topography based on laser excitation. The principle of the LSFM consists of a planar illumination of a 3d sample by means of a sheet-shaped light beam. The layer-by-layer illumination and detection of the emitting signal reduces photobleaching and tomographic imaging in z-direction allows the visualization of a whole volume.[13] The penetration depth of the light sheet depends on scattering of light within the biological tissue. To increase the penetration, a chemical clearing has to be applied in order to enhance tissue transparency. This is achieved in particular by adjusting the tissue-specific refractive indices[14] using, for example, organic solvents like benzyl alcohol/benzyl benzoate (BABB) to image whole organs.[15] Using this microscopic technique after fluorescent antibody/nanobody penetration through the specimen, functional analyses of specific proteins in single cells can be realized, for example, to gain insights into the 3d morphology of murine lungs.[16] In addition, LFSM has shown its outstanding value in the examination of tumor specimens and their interaction with the surrounding environment in 3d with or without fluorescent label.[17,18]

Therefore, the aim of this study was to visualize the 3d structure of the murine male reproductive organ using LSFM without any use of exogenous stains. With this label-free imaging approach, we achieved by autofluorescence detailed morphological insights into the entire organ with its convoluted connections and junctions of these extensive

duct systems due to its manifold intrinsic fluorescence properties. The autofluorescence of the organ led to a clear, unambiguous assignment of the characteristic, and unique features of the testis itself, the efferent duct and vas deferens as well as the pampiniform plexus and the epididymis in a cellular resolution.

2 | MATERIAL AND METHODS

2.1 | Animals

C57BL6/J mice (male; age 4–9 months) obtained from the animal facility of the University Medical Center Gttingen and Rj:*NMRI-Foxn1*$^{nu/nu}$ mice (male; age: 4–14 months) obtained from Janvier Labs, France were kept under 12:12h dark:light cycle with ad libitum access to food and water. All animals were sacrificed using an overdose of carbon dioxide (CO_2), followed by cervical dislocation. The testes were removed and immediately transferred into the fixative.

2.2 | Ethics statement

All animal experimental procedures were performed in compliance with the European (2010/63/EU) and German regulations on Animal Welfare and were approved by the administration of Lower Saxony (LAVES) (Nr. 33.9-42502-04-17.2742, T 10/16).

2.3 | Sample preparation

In order to prepare the tissue samples for further LSFM imaging, we generally followed the protocol for dehydration and sample preparation of the LSFM distributor Miltenyi biotec Ltd (https://www.miltenyibiotec.com/DE-en/applications/all-protocols/immunostaining-and-clearing-of-mouse-brain-hemispheres-for-3d-imaging-analysis-1.html). The excised entire testis was directly fixed after removal for 24 h with different fixatives: either with paraformaldehyde (PFA) 4% in phosphate-buffered saline (PBS), Davidson's fixative, 37% (DF37; three parts ethanol, one part glacial acetic acid, two parts 37% formalin, three parts tap water), Davidson's fixative, 10% (DF10; three parts ethanol, one part glacial acetic acid, two parts 10% formalin, three parts tap water) or modified Davidson's fixative (mDF37; three parts ethanol, one part glacial acetic acid, six parts formalin 37%, 10 parts tap water). After a sufficient washing step with PBS, the samples were dehydrated with ascending ethanol series: (30% ethanol for 4 h, 50% ethanol for 4 h, 70% ethanol for 12 h, 90% ethanol for 4 h, 100% ethanol for 4 h, 100% ethanol for 12 h). Afterward the dehydrated testis was incubated in BABB (one part benzyl alcohol, two parts benzyl benzoate) solution by gently shaking the sample at room temperature to clear the tissue for at least up to 16 days until sufficient tissue transparency was achieved at a uniform refractive index to prevent light scattering and light absorption. The samples were either kept in BABB solution at 4°C or embedded in paraffin for further histological validation.

TABLE 1 List of all laser bandpath filter combinations used for LSFM data acquisition

Excitation wave length in nm	Emission wave length in nm
470/30	525/50
520/40	585/40
595/20	690/50
710/75	810/90

2.4 | Light sheet fluorescence microscopy

The completely cleared murine testes were analyzed by using the UltraMicroscope II LSFM (UM II) and/or the follow-up device UltraMicroscope Blaze LSFM (Miltenyi Biotec, Germany). The specimens were attached to the sample holder, allowing a sample size of 1 cm^3, either by a screw or with superglue. For the LSFM scanning procedure, they were placed into the ethyl cinnamate (ECI) filled cuvette, which was used as noncorrosive alternative to BABB with comparable refractive index. Fluorescence excitation was done via NKT SuperK Extreme white light laser of 0.6 W visible power (NKT Photonics, Denmark). The images were acquired by using the software *ImSpector 7*. The detection part of the LSFM comprises the objectives (2×, 4×) and filter sets, equipped with custom made modulators to compensate refractive index mismatch and an optical band pass filter (49 nm full bandwidth centered at ± 550 nm). Both LSFMs are equipped with a sCMOS camera, 4.2 megapixel with 2048 × 2048 pixel resolution (PCO, Germany). The used corresponding filter sets are listed in Table 1. The software arivis Vision 4D (arivis, Germany) was applied for data analysis.

2.5 | 2D histology, fluorescence image acquisition, and processing

After LFSM scan, the testes were further processed for histological analyses. Paraffin embedded testes were cut into 2 μm sections and stained as described before, with either haematoxylin/eosin (H&E) for light microscopy or stained with DAPI as nuclear stain for planar fluorescence microscopy.[19]

Endothelial staining was performed with a rabbit polyclonal antibody directed against the endothelial cell marker CD31 (abcam, 28364) at 4°C overnight. Subsequently, sections were incubated with an antirabbit secondary antibody (Histofine, Nichirei Bioscience, 414142F) for 30 min at room temperature.

Fluorescent images were taking using a fluorescence microscope (BX63, Olympus, Tokyo, Japan) equipped with a digital camera (CP80, Olympus, Tokyo, Japan) and a motorized scanning stage (BX3-SSU,

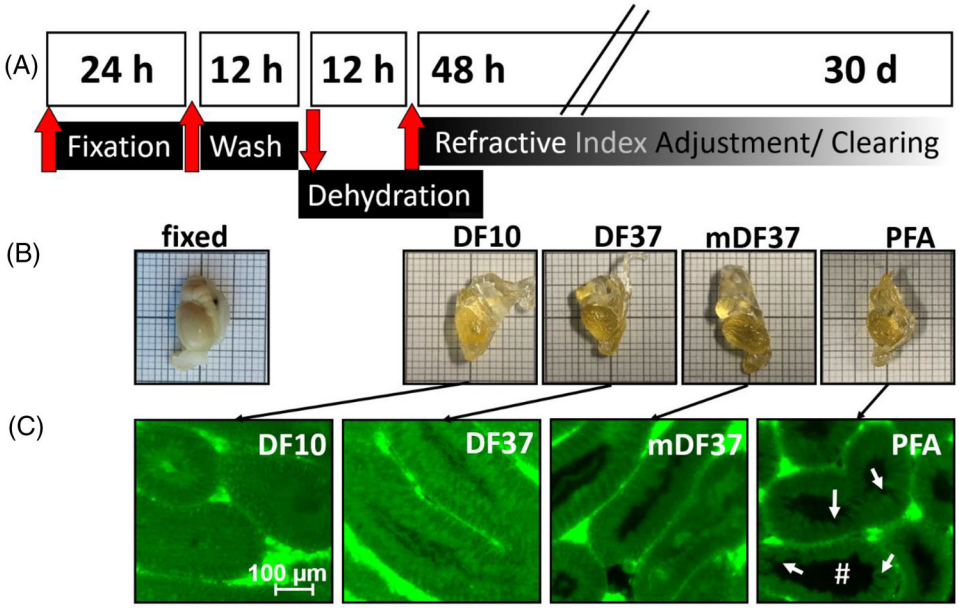

FIGURE 1 **The workflow of tissue preparation for 3d light sheet fluorescence microscopy (LSFM) imaging.** (**A**) The tissue preparation for 3d LSFM imaging started with the fixation, followed by a washing step, a dehydration analogous to conventional histology and at last the clearing process using benzoic acid/benzyl benzoate (BABB). (B) To develop the optimal preparation process for the testis samples, four different fixatives were applied in an experimental approach: Davidson's fixative 10 (DF10), Davidson's fixative 37 (DF37), modified Davidson's fixative 37 (mDF37), and 4% paraformaldehyde (PFA). Independent of the fixative, after BABB clearing all tissue samples were transparent, allowing a complete laser penetration during the LSFM scan. (C) LSFM fluorescence images show that all fixatives used did not alter the intrinsic fluorescence in the LSFM data sets, but PFA led to alterations of the tissue. Clearly visible are artificially expanded lumina (#) and loss of tight junctions (arrows) within the germinal epithelium in the PFA fluorescence data set in comparison to all DF fixatives.

Olympus, Tokyo, Japan) with 100× magnification. Images were analyzed using CellSens Software v.2.3 (Olympus, Tokyo, Japan).

3 | RESULTS

3.1 | LSFM imaging requires a sufficient sample preparation and clearing

Murine testes samples of two different mouse strains were used to evaluate the feasibility of the preparation workflow and to study the autofluorescence of this tissue type by 3d LSFM imaging (Figure 1A).

In order to assess the influence of the fixation method on the tissue specific autofluorescence of the testes during the process of LSFM preparation, four groups of testes were transferred immediately after collection either to 4% PFA, to 10% Davidson's fixative (DF10), to 37% Davidson's fixative (DF37) or to modified 37% Davidson's fixative (m37DF) and fixed overnight. Washing and dehydration were subsequently performed referring to the standard protocol as well as clearing of the tissue applying BABB (Figure 1B), which was also used as storage solution. By visual inspection after at least 16 days, all samples were invisible in the BABB solution, showing therefore the same refractive index like BABB, independent of the fixative used.

The intact and transparent tissue samples were scanned individually using LSFM. Different filter combinations for the *white light laser* (Table 1) were applied to detect autofluorescence phenomena throughout the volume of the testis.

All data sets of 3d LSFM of the testes showed comparable autofluorescence signals, independent of the fixation used (Figure 1C). Both, the intensity of the fluorescence and the morphological specificity of the signal did not reveal any differences between the three Davidson fixatives tested. However, the use of PFA resulted in a change in tissue integrity and caused the artificial dilatation of lumina of the tubules and loss of tight junctions of the *Sertoli cells* in germinal epithelium (Figure 1C). Subsequent conventional planar histology on H&E sections confirmed the disintegrated tight junctions in the germinal epithelium in fixed samples (data not shown). PFA was therefore not suitable for fixation of the reproductive organ and should be replaced by alternative fixatives, although the autofluorescence properties of the tissue were not affected by PFA fixation. Due to the handling and the preparation of the fixative, further tissue fixation was performed using 37% Davidson's fixative.

3.2 | LSFM data sets represent the 3d structure of the testis in its entirety

For 3d depiction of the whole organ, LSFM data sets were generated by tomographic slice images of 5 μm thickness for every used filter set combination. Out of this data set, a volume rendering was applied leading to a 3d visualization in arbitrary planes (Figure 2A, upper panel).

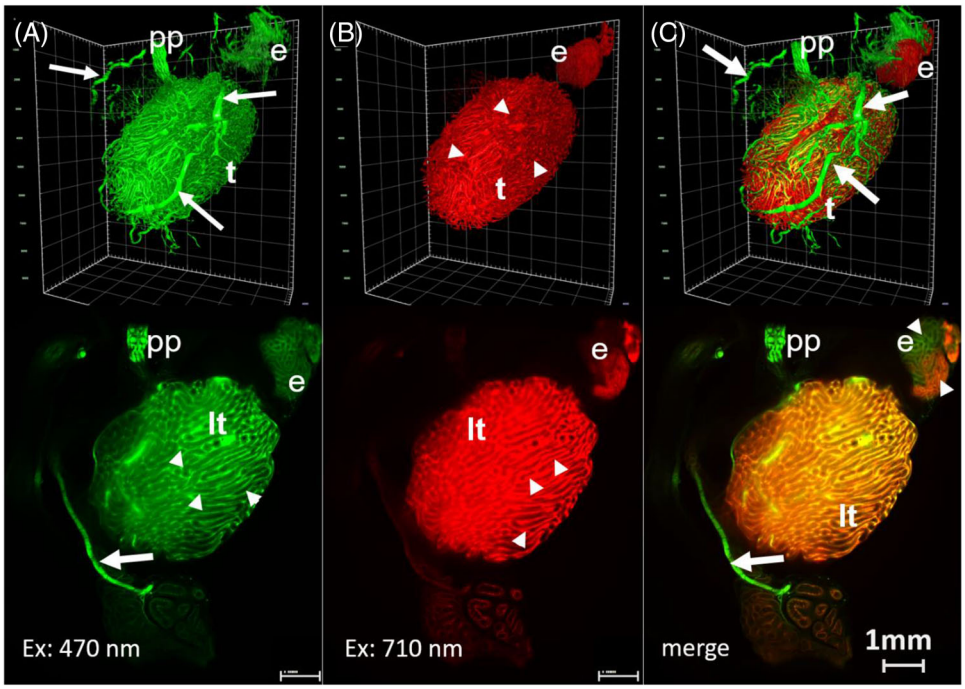

FIGURE 2 **Representative 3d images of a UM II light sheet fluorescence microscopy (LSFM) data set of an entire murine testis**. Depending on the LSFM filter sets used different anatomical structures of the unlabeled, cleared testis (t) can be depicted. (A) blood vessels (ex: 470/30 nm; em: 525/50 nm, arrows), in particular of the pampiniform plexus (pp) are visible in 3d (upper panel) and in tomographic sections in 2d (lower panel). In addition, basal membranes from the *lobuli testis* (lt, arrow heads) within the testis and the epididymis (e) are visible. (B) The epithelia and lumina of the *lobuli testis* (arrow heads) can be represented by a filter set for a long wave length range (ex: 710/75 nm; em: 810/90 nm) in 3d (upper panel) and 2d (lower panel). Fluorescence can also be detected in defined areas of the *caput epididymidis* (e) in 3d and 2d. (C) Images composed of both filter sets are shown in 3d and 2d combining the information of the peripheral blood supply of the testis (arrows) and the pampiniform plexus (pp) as well as of the *lobuli testis* (lt). Remarkable is the clear discrimination of two morphological portions within the *caput epididymidis* (e) exhibiting different fluorescent emission (arrow heads).

Depending on the filter sets used, the anatomical characteristics of the testis and adjacent structures could already be mapped in the image of the entire sample volume. As shown in Figure 2, peripheral blood vessels below the *tunica albuginea* and vessels of the pampiniform plexus were visualized at low wavelengths, with excitation of 470 nm and emission of 525 nm.

In 2d sections of the same testis, the basement membranes of the seminiferous tubules and portions of the caput epididymidis could be visualized more precisely after subtraction of the strong fluorescent peripheral blood vessels whereas the lumina appeared always black in LFSM (Figure 2A, lower panel).

In contrast, images of the filter set: excitation at 715 nm and emission of 810 nm accentuated more lumina and epithelium of the seminiferous tubules and epididymis (Figure 2B). In this wavelength range, blood vessels could not be identified. A composition of both wavelength ranges into one image gave a comprehensive overview of the entire testis with a clear assignment of the autofluorescence signals to the portions of the blood supply and the testicular lobules (Figure 2C). In the *caput epididymidis* signals of both wavelength ranges resulted in nonoverlapping signals (Figure 2C). Thus, the LSFM scan with different filter sets of the entire mouse testis allowed visualization in all angles and virtual sectional planes and the assignment of adjacent structures by specific autofluorescence signals.

In order to gain information on a microscopic level, the 4× objective was used, to analyze testes from BL/6 and NMRI nu/nu mice by LFSM at high resolution. All data sets were generated by a combination of filter sets: ex: 520/40 nm; em: 585/40 nm (green), ex: 710/75 nm; em: 810/90 nm (red).

Focusing at specified regions of interest within the testes allowed the accurate visualization of the *lobuli testis* with the seminiferous tubules (Figure 3A) in the green wavelength range. Even supplying capillaries surrounding the tubules were visible by LSFM. The evaluation of the regional differences in height of the germinal epithelium was possible due to the clear delineation of the luminal diameter within the tubules. Regions of intense fluorescence in the red wavelength range were associated to accumulations of *Leydig cells*. A 3d data set revealed the dense meshwork of the convoluted, small tubules (Figure 3A, right). As prominent adjacent structure of the testis, the spermatic cord and its peripheral blood vessels were obtained in multiple sections and represented therefore the vas deferens as winding, muscular hollow organ (Figure 3B) in the green wavelength range. At a higher magnification, this also revealed the stratification of the vas deferens (Figure 3B) from the sperm containing lumen to the differentially orientated muscle layers and the blood vessel containing adventitia.

Furthermore, a noteworthy convolute of blood vessels that supply the testis is the pampiniform plexus. These tortuous bundles of veins

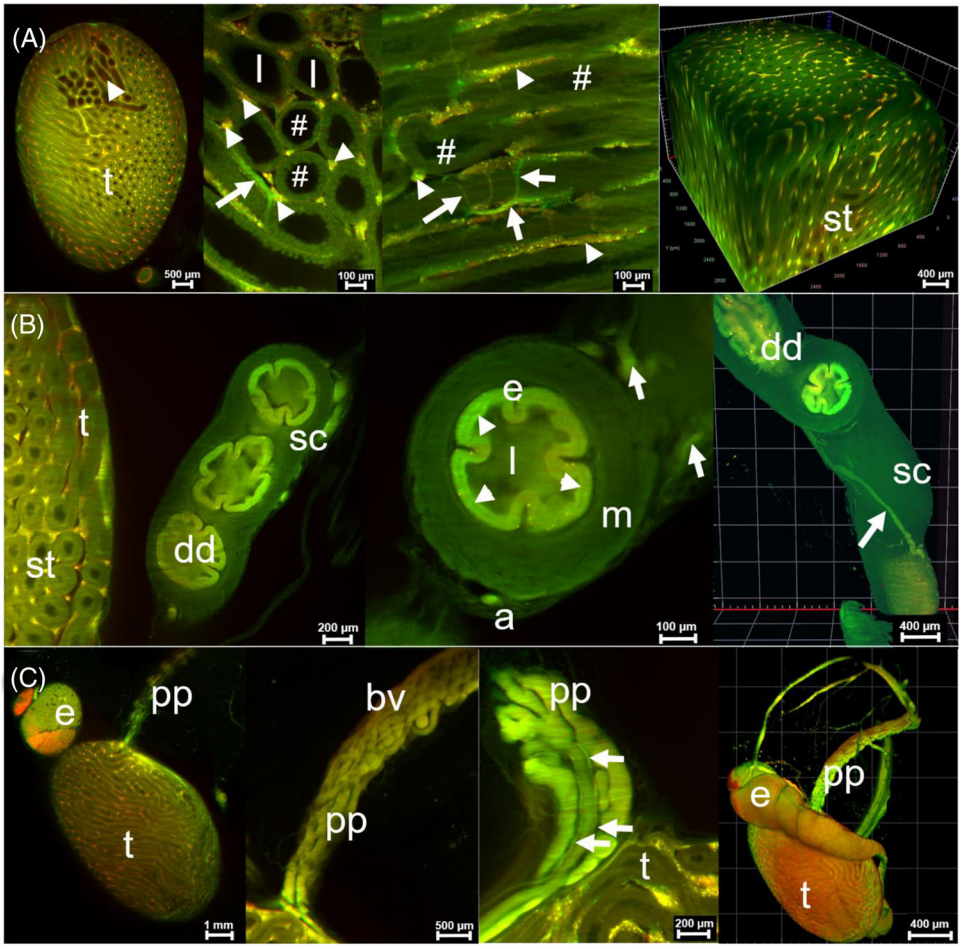

FIGURE 3 **Unlabeled UM Blaze light sheet fluorescence microscopy (LSFM) generated data sets provide a comprehensive virtual histology of the murine testis. (A)** Specific signals from intrinsic fluorescence allow clear identification of the seminiferous tubules (st) within the testis (t) in 2d and 3d (right). Note the variable luminal (l) space (#) within the germinal epithelium, and the strong autofluorescence of the *Leydig cells* (arrow heads) and the tubule-surrounding capillaries (arrows). **(B)** 2d and 3d (right) visualizations of the spermatic cord (sc) with the vas deferens (dd) in various sections demonstrate in detail the stratification of this hollow organ: the narrow, star shaped lumen (l), a stratified epithelium (e) with clearly visible two layers (arrow heads), the smooth muscle formations (m) in different orientations and blood vessel (arrows) containing adventitia. **(C)** Both the testicular blood supply and discharge is shown. The pampiniform plexus (pp) is connected to the testis and contains multiple, tortuous blood vessels (bv). At a higher magnification, even the vessel wall (arrows) is visible in the label-free sections. The 3d depiction of the pampiniform plexus revealed its anatomical relation to the testis (t) and the epididymis (e). All images were composed of a combination of filter sets: ex: 520/40 nm; em: 585/40 nm (green), ex: 710/75 nm; em: 810/90 nm (red).

were traced starting from the outside of the testis to the direction of the spermatic cord, mostly accentuated within the green wavelength range (Figure 3C). Even the endothelial walls of the blood vessels could be evaluated in detail by visualizing several cross sections of this venous plexus.

3.3 | Epididymis and efferent ducts can be discriminated directly by their intrinsic fluorescence

Since the LSFM data sets from murine male reproductive organs showed clearly differences in the intrinsic fluorescence within the *caput epididymidis*, this region was analyzed in more detail. While after laser excitation the efferent ducts of testis up to the junction of epididymis emit long wavelength red light, the directly adjacent initial portion of the *caput epididymidis* emits short wavelength light in the green range (Figure 4). This observation was independent of the mouse strain.

As a connection between the testis and the epididymal duct, four to six individual efferent ducts in the mouse join to form an efferent common duct that merges with the caput of the epididymis, which was shown clearly by autofluorescence in the 3d data sets (Figure 4A, right).

In order to distinguish the convolute of efferent ducts and the caput of the epididymis by their characteristic highest fluorescence intensity, two filter sets were used. The filter combination ex: 710/75 nm and em: 810/90 nm was applied to assess the efferent ducts, and the filter combination ex: 520/40 nm and em: 585/40 nm was used to

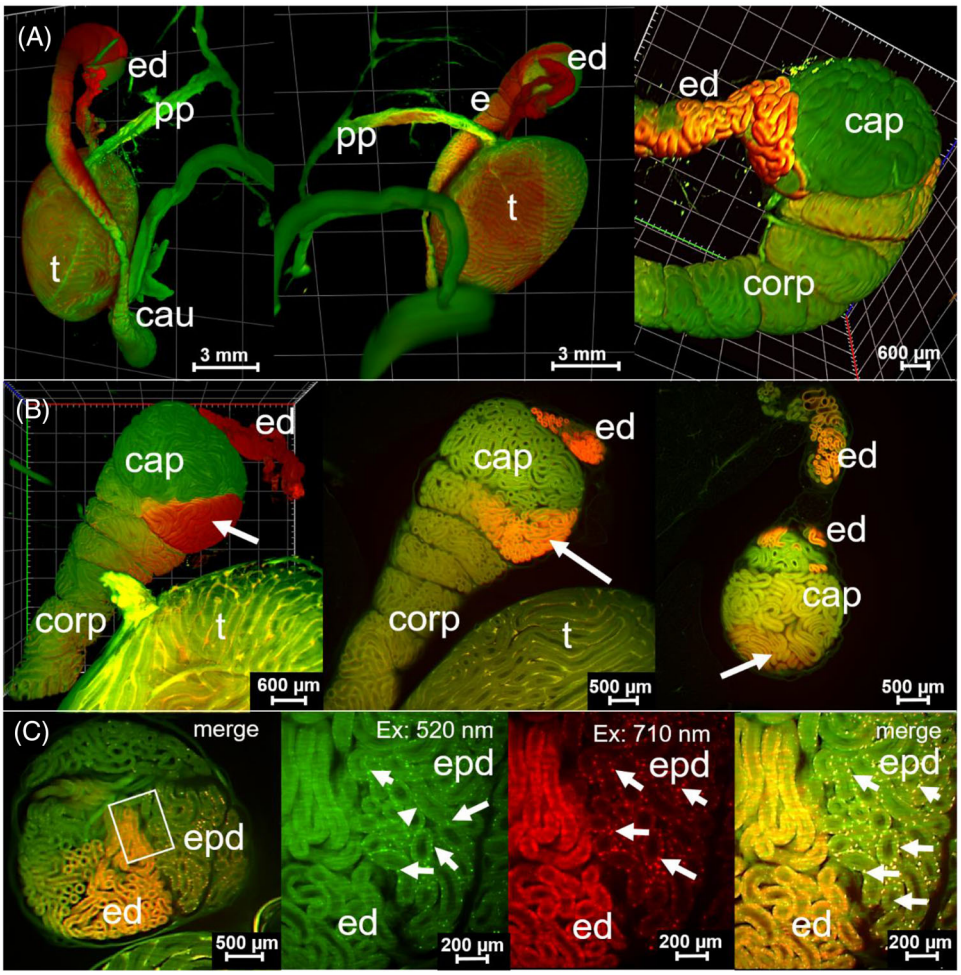

FIGURE 4 **The use of different filter sets in the UM Blaze light sheet fluorescence microscopy (LSFM) allows unambiguous identification of the efferent duct/ epididymal junction**. **(A)** 3d views of three murine testes from Bl/6 mice show clear delineating autofluorescence signals in the region of the junction of the efferent ducts (ed) and the *caput epididymidis* (cap). The initial portion of the epididymis, the corpus (corp) and caudal portion (cau), large parts of the testis (t), and blood vessels of the pampiniform plexus (pp) were visualized in the low wavelength range in green (ex: 520/40 nm; em: 585/40 nm). In contrast, the terminal efferent ducts (ed) exhibit a strong autofluorescence (in red) at the filter combination ex: 710/75 nm; em: 810/90 nm. All three images were composed of a combination of both filter sets. **(B)** With a direct focus on the epididymal duct, the caput (cap) and corpus (corp) of the epididymis in 3d (left) and 2d (middle, right) showed that the emitted fluorescence of the terminal efferent ducts in red can be clearly differentiated from the initial *caput epididymidis* in green. However, areas within the caput also showed autofluorescence in the long wavelength range (arrow), while some segments of the caput and corpus contained a color mixture of red and green components (yellow). All three images were composed of a combination of filter sets: ex: 520/40 nm; em 585/40 nm (green), ex: 710/75 nm; em: 810/90 nm (red). **(C)** By a direct comparison of efferent ducts (ed) with the multiple convoluted epididymal duct in both color channels, the autofluorescence signals of the efferent ducts could be assigned to the entire cytoplasm of the epithelium (left). Note that by higher magnification strong autofluorescent basal cell inclusions were observed in the cytoplasm of the epithelium of the epididymal duct (epd, arrows), which were visible in all filter combinations and in the merged images (right). All three images were composed like indicated using the filter sets: ex: 520/40 nm; em 585/40 nm (green), ex: 710/75 nm; em: 810/90 nm (red).

visualize the epididymis (Figure 4B,C). A higher magnification of a sectional image at the interface between the efferent ducts and the epididymis revealed nearly uniform cytoplasmic autofluorescence of the multiple tortuous sections of the main efferent duct (Figure 4C). Because of this strong intrinsic fluorescence, the adjacent ductal lumina were difficult to determine. In the area of the basal cell row, subcellular, granular inclusions with a strong intrinsic fluorescence in the direction of the basement membrane were visualized in both filter combinations. They correspond most likely to protein aggregates or lipofuscin granules. In contrast, the epithelial cells of the epididymis could only be detected in the short wavelength range. Excitation in the near-infrared range resulted only in the visualization of basal cytoplasmic inclusions, which are not nuclei.

Thus, label-free LSFM in combination with the use of different filter sets offers the possibility to discriminate and evaluate even structures close to each other, like the junction of terminal efferent ducts and the initial epididymal duct, based only on their autofluorescence properties (Figure 4C).

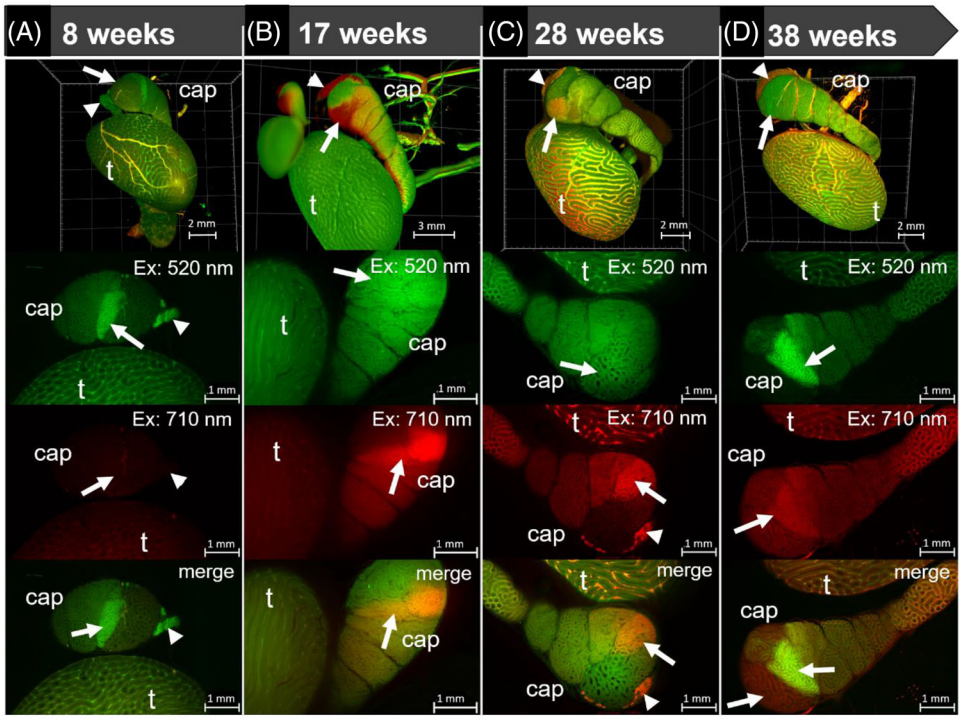

FIGURE 5 **The fluorescent properties of the efferent duct/epididymal junction are age dependent. (A–D)** 3d and 2d views of murine testes from Bl/6 mice of four different ages (8–38 weeks), analyzed by light sheet fluorescence microscopy (LSFM) show different patterns of autofluorescence signals in the region of the *caput epididymidis* (cap). **(A)** Whereas all structures of the initial portion of the terminal efferent ducts (arrow heads) and the epididymis (arrows) in 8 weeks old mice were visualized solely in the low wavelength range in green. **(B and C)** The terminal efferent ducts and parts of the *caput epididymidis* (arrows) in 17 and 28 weeks old mice exhibit a clear delineation due to the strong autofluorescence in red and green in 3d and 2d images. **(D)** The 3d and 2d images of the testis of a 38 weeks old mouse show a decrease in autofluorescence in the *caput epididymidis* area (arrow) compared to the 28 weeks old mice. All images were composed like indicated using the filter sets: ex: 520/40 nm; em 585/40 nm (green), ex: 710/75 nm; em: 810/90 nm (red). Merged images were composed of a combination of both filter sets.

The autofluorescence of the efferent duct/ epididymal junction showed clear differences depending on the age of the mice (Figure 5). To analyze this correlation, the reproductive organs of at least three Bl/6 mice each were examined at the ages of 8 weeks, 17 weeks, 28 weeks, and 38 weeks using LSFM. Only in the data sets of 17 weeks and older mice did a distinct intrinsic fluorescence occur in the red, longer wavelength region, which was allocated to the efferent duct and parts of the caput epididymidis (Figure 5B,C).

These red components were not observed in the 8 weeks old mice (Figure 5A). The data further suggest that the longer wavelength fluorescence may decrease with age, as shown by the image data from the 38 weeks old mice (Figure 5D).

3.4 | 2d fluorescence microscopy and conventional histology confirm the information of LSFM generated data sets

To confirm the identified morphological structures of the testes obtained by 3d LSFM, histological sections of the cleared testes were prepared for planar light microscopy using H&E sections and fluorescence microscopy using native unlabeled sections and DAPI sections (Figure 6A). The ductal structure of seminiferous tubules and the blood vessels with their basement membranes were clearly visible in the unlabeled native sections. Moreover, within the germinal epithelium cytoplasmic extensions of the *Sertoli cells* were detected (Figure 6A, left) and confirmed in H&E stained sections (Figure 6A, middle). This observation was not possible by the analysis of LSFM data alone due to the lower resolution than planar fluorescence microscopy. Like in LSFM, *Leydig cell* accumulations revealed strong fluorescent signals (Figure 6A). Nuclei of the germinal epithelium and endothelium of surrounding blood vessels, as well as nuclei of *Leydig cells* around the tubules were only detected by H&E or DAPI stain (Figure 6A, middle, right).

The higher magnification of the unlabeled sections analyzed by planar fluorescence microscopy showed basally located cytoplasmatic inclusions within the epithelial periphery of the efferent ducts (Figure 6B). Due to the resolution limit of the LSFM, this layer of fluorescent granules was imaged as a homogeneous cytoplasmic fluorescence in LSFM data sets, which provided a sharp morphological separation from the epididymal epithelium (Figure 4C). Histological analyses of an H&E stain of the adjacent paraffin section showed the sperm filled ducts as well as the two layered epithelium of the efferent ducts, confirming the assumption of the epithelial cytoplasmic origin

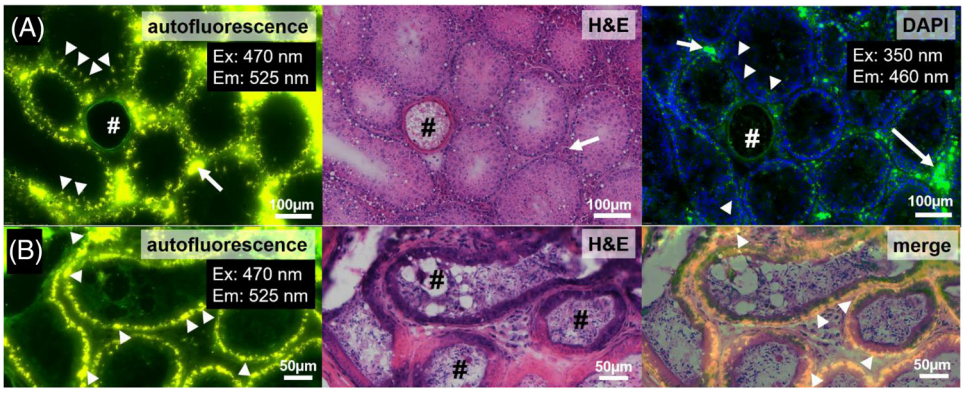

FIGURE 6 **Alignment of testicular structures depicted by planar fluorescence microscopy with conventional histology. (A)** A tissue section of the light sheet fluorescence microscopy (LSFM) scanned testis without additional staining shows a strong intrinsic fluorescence in the area of seminal tubules by the use of planar fluorescence microscopy. Allocated autofluorescent structures represent the cytoplasm of *Sertoli cells* (arrow heads) as well as the highly fluorescent *Leydig cell* accumulations (arrow) and the wall of a blood vessel (#). Histological analysis of adjacent H&E stained tissue sections in light microscopy and a DAPI-stained section in fluorescence microscopy confirmed presence of these structures. **(B)** In the region of the efferent ducts, the fluorescence images of a planar unlabeled section represent granular fluorescent structures (arrow heads). Assigned to the epithelial cytoplasm, the fluorescence was particularly noticeable in the ductal periphery. Images of the H&E stained section clearly shows the sperm filled ducts (#) and the surrounding epithelium. An overlay of both image data (right) revealed a localization of the signals (arrow heads) within the basal cells of the ducts. In contrast, the sperm and the connective tissue showed no fluorescence. All fluorescence microscopy images were composed of a combination of filter sets: ex: 470 nm; em 525 nm (yellow/green), ex: 350 nm; em: 460 nm (DAPI/blue).

of the fluorescent granules (Figure 6B, middle). An overlay of the planar fluorescence and the H&E images revealed a clear localization of the fluorescence within the basal cells of the duct epithelium. In contrast, the sperm and the connective tissue showed no fluorescence (Figure 6B, right).

The combination of label-free 3d LSFM microscopy together with subcellular resolution of subsequent histological analysis of murine testes offered therefore a comprehensive look, combining the visualization of the entire organ, at a glance, and fine structured morphological aspects in detail (Figure 7). Although the resolution of LSFM data sets is currently inferior to planar microscopy, the 3d microscopic approach accurately depicted the tubules and ductal structures of the testes in their anatomical relation to adjacent morphological portions of the reproductive system (Figure 7A). Tomographic slices of the virtual data set gave insight into this complex organ, with its epithelial organization, the blood vessel supply from capillaries to the venous plexus and an additional functional aspect. Based on the presence and exact location of fluorescent cellular inclusions, metabolite-containing vacuoles or the filling level of sperm in the ductal portions (Figures 4C and 7B) could be evaluated, hollow structures like the spermatic cord were assessable through the entire volume, and the height of the germinal epithelium could be determined in all three dimensions (Figures 3A and 7B). The correct identification of the morphological structures like blood vessels, the *tunica albuginea*, the vas deferens with the spermatic cord as well as the epididymis was confirmed by conventional histology (Figure 7C–E). Anti-CD31 antibody staining showed a positive and specific labelling of endothelial cells in testicular vessels (Figure 7D,E), demonstrating that a subsequent IHC approach is possible without changes in pretreatment or staining protocols after BABB clearing procedure.

4 | DISCUSSION

The multifaceted functions of the male reproductive organ are reflected in its highly complex morphological composition of convoluted tubules and ducts. Although many aspects of testicular histology have been known ultrastructurally for decades by planar microscopy and electron microscopy,[20] the intricate interplay of the individual ductal components has rarely been shown in three dimensions. The present study demonstrates the feasibility of an ex vivo LSFM examination in combination with a clearing protocol, developed for this purpose, to assess for the first time the murine testis label-free either in its entirety at all possible angles in 3d or as a sequential tomographic data set. The presence of intrinsic fluorophores such as collagen, elastin, myoglobin, haemoglobin, and others leads to specific autofluorescence signals within the testis thereby enabling the clear distinction of anatomical structures of the testis and deferent structures by LFSM. Thus, label-free LSFM in combination with different filter sets allows accurate qualitative assessment of the testis, in particular its individual morphological structures down to a cytoplasmatic level as validated by subsequent 2d histology. We show that visualization of blood vessels and seminal ducts as well as the germinal epithelium, and accumulations of *Leydig cells* is possible without any doubt due to their specific intrinsic fluorescence profile. In this study, we report a clear delineation of the lumina within the seminiferous tubules, the basement membrane, and the height of the germinal epithelium by LSFM. This epithelial height is a hallmark of functional spermatogenesis. Age-related involution[21] anatomical malformations like cryptorchidism[22] or drug effects[23] lead to degenerative changes in the germinal epithelium. They are important histomorphological parameters for the pathological assessment of a testicular biopsy.[6] The

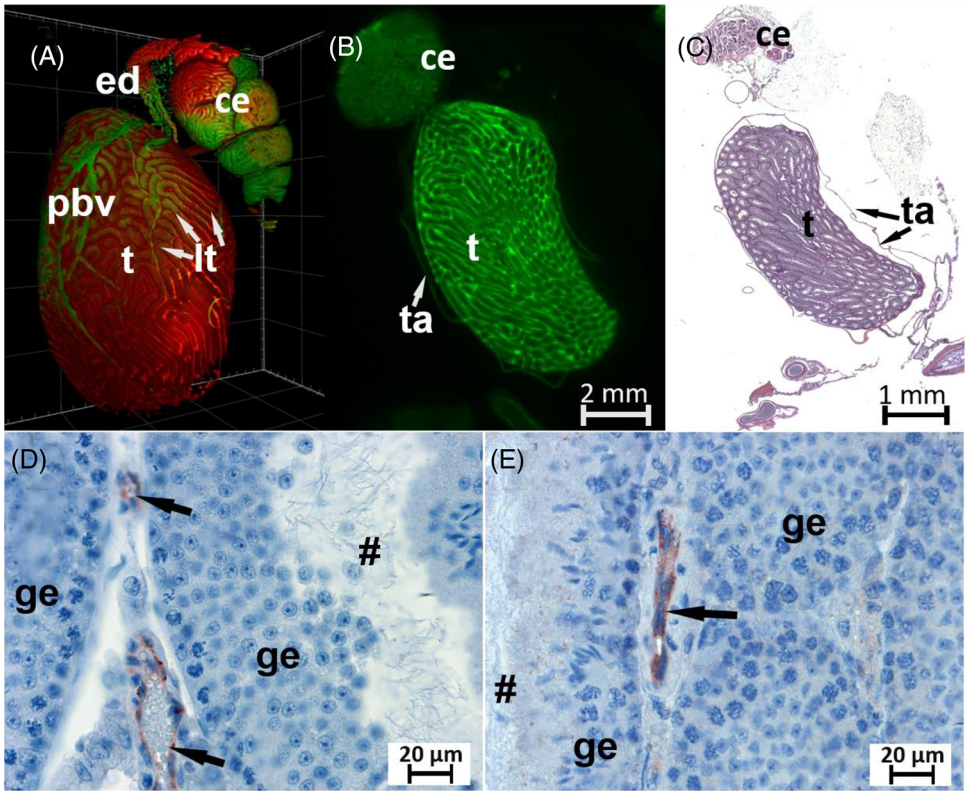

FIGURE 7 **3d versus tomographic UM II light sheet fluorescence microscopy (LSFM) data sets of the unlabeled testis depicts its entire morphology at a glance**. **(A)** The compact structure of the entire testis (t) with its *lobuli testis* (lt), peripheral blood vessels (pbv), the efferent ducts (ed), and the *caput epididymidis* (ce) visualized in 3d could be represented in their correct anatomical relation, and in all arbitrary angles. The image was composed using the filter sets: ex: 520/40 nm; em 585/40 nm (green), ex: 710/75 nm; em: 810/90 nm (red). **(B)** A virtual tomographic section of the same data set allowed the visualization of convoluted ducts and tubules with their lumina, but also the connective tissue of the *tunica albuginea* (ta, arrows) within the entire volume of the testis and without any additional staining. The image was generated using the filter set: ex: 520/40 nm; em 585/40 nm (green). **(C)** The conventional H&E staining of a single slice of the testis and adjacent structures contained the same planar information like in (B) but is restricted to one plane. (D and E) A consecutive IHC approach after LSFM analysis, using a CD31 antibody shows the specific binding to endothelial cells (arrows) in the periphery of seminal tubules with germinal endothelium (ge) and luminal space (#). Therefore, it confirms the successful applicability of IHC to native paraffinized **(D)** and benzyl alcohol/benzyl benzoate (BABB) cleared and paraffinized **(E)** testicular tissue.

3d assessment of the entire testicular volume, presented in this study, has shown to accurately spatially assess the morphology from the *lobuli testis* through the epididymis to the *ductus deferens* and the draining vessels of the pampiniform plexus at microscopic resolution. In comparison, even planar sections of the autofluorescent testis only show the complex structures and the interplay of ducts and tubules of the testis inadequately in isolated micrographs.[24]

Here, we demonstrate that the junction of efferent ducts and the *caput epididymidis* can be visualized with LSFM due to the outstanding difference in the autofluorescence signals of both structures. The efferent ducts are visualized as a bundled duct convolute in the long wave autofluorescence range. The epididymis itself appears in the LSFM data sets as segmented convolute of a winded duct with a clear assignment of caput, corpus, and cauda, distinguishable by their different autofluorescence properties. The intrinsic fluorescence depends on age and therefore most likely on sexual maturity and activity. The epithelia of efferent ducts and epididymal duct are histologically distinct and have different functions reflected in their specific transcriptome,[7] expressing proteins with different intrinsic fluorescence. In particular, the function of estrogen regulated water reabsorption[25] within the efferent ducts could lead to the characteristic autofluorescence of the basal cell inclusions within the epithelium observed in our study. Typical features of the tubules of the *caput epididymidis* are the wide lumina and stereocilia that retain the sperm for maturation, which are also depicted here by LFSM. Toward the *cauda epididymidis*, the sperm reservoir function increases in importance. A recent study found that not only efferent ducts and proximal epididymis differ in their gene expression, but also the regions of the caput and *cauda epididymidis*,[26] resulting in different protein expression patterns and thus in distinct fluorescent visualization. Different autofluorescence behaviors of testicular structures may thus also be indicative of functional alterations and will be the subject of further research. The potential of label-free virtual histology using LSFM has been already demonstrated in a variety of studies for 3d imaging of organs such as human skin biopsy[14] and of murine lung, with and without application of fluorescent nanoparticles.[16] Likewise, in our

study, although unstained intact biopsies and specimens were used, the tissue composition within the entire volume could be identified. The mesoscopic imaging approach of the human pancreas with its islets of Langerhans and tumorous areas in specimen of pancreatic ductal adenocarcinoma by Hahn et al., 2020[17] demonstrated that pathological tissue has characteristic altered intrinsic fluorescence signals, which can therefore be used to detect the tumorous microenvironment and the tumor margin. The exact knowledge of the structural morphology and specific autofluorescence of the healthy tissue of the male reproductive organ as depicted in this study is therefore an important prerequisite for the evaluation of the pathologically altered testis.

An excellent but technically complex method to visualize morphological alterations of the developing and aging testis is the 3d reconstruction of sequentially taken histological slices.[27–29] Furthermore, even discrete structural alterations of the entire male reproductive organ were traced spatially and quantified in comparative interspecies studies, using this technique.[30] Thereby, the advantage of complete 3d data sets of the testis generated either by LSFM or after later reconstruction is to address a number of preclinical questions. For example, by visualizing the entire testis alterations in spermatogenesis in genetically modified mice could be assessed in 3d comprehensively, and their study would not be limited to classical 2d histological/immunofluorescence methods.[31,32] Studies on the influence of environmental toxins[33] or drugs[34] on spermatogenesis are also of great preclinical interest. In addition to animal experiments, however, innovative 3d testicular scaffold-based approaches to model a testicular microenvironment in vitro also exist in this regard.[35] The LFSM-based 3d analysis of the entire scaffold would be an innovative approach to reproduce different types of infertility. This is of special interest, since infertility is a common and increasing challenge in the western world and is due to the male in about 50% of cases.[6,36] In the future, 3d LSFM analysis of testicular biopsies, used in the clinic to diagnose male infertility, offers the possibility of a label-free, complex assessment of the entire 3d biopsy volume. LSFM has the potential to detect distinct structural alterations of the testis, such as thickening of the *tunica albuginea*, vacuolization of the seminiferous epithelium, widening of interstitial spaces, atrophic tubules, and fibrosis.[37] The intrinsic fluorescence of typical testicular structures such as *Leydig cells* and the basement membranes of seminiferous tubules were already visualized in 2d fluorescence studies.[24] Since the amount and distribution of these endocrine cells is of particular histopathological importance,[6] the 3d assessment of the entirety of *Leydig cell* clusters within the testis could be an ideal diagnostic application of LSFM.

At the same time, subsequent histological and immunohistochemical analyses of the tissues are easily possible, which was confirmed by a consecutive H&E and anti-CD31 antibody staining. This offers important details on the cellular morphology of the analyzed tissue. Both approaches, 2d and 3d microscopy, can be conducted on the same sample and one does not exclude the other. Especially in pathological conditions, labeling of different type of germ cells is critical for the evaluation of spermatogenesis. Therefore, LSFM with its partially subcellular resolution might be combined with the planar microscopy to get more comprehensive data of the testis.

The present study shows that fixation with PFA has a lasting effect on tissue integrity of the testis. In particular, cell–cell contacts widened after application of PFA fixative and resulted in superficial cell sloughing into the lumen within the seminiferous tubules. Although PFA did not change the autofluorescence pattern of, for example, *Leydig cells* or cell membranes, the nuclear and cytoplasmic granularity increased after PFA fixation compared to results obtained with Davidson's fixative of different concentration. Similar effects were observed by others when using a standard formalin fixation compared to Bouin's solution as fixative,[38] which together with our results demonstrates that careful tissue preparation especially the fixative is an important prerequisite for high quality datasets of the testis.

In summary, this study shows that 3d virtual histology of the male reproductive organ of the mouse is feasible using a straightforward preparation protocol with gentle tissue fixation. Thus, clinical translation of the 3d LSFM method for assessment of testis biopsies with altered tissue structures and cellular organizations is feasible and may lead to new insights into testicular development and pathological alterations of this complex organ.

AUTHOR CONTRIBUTIONS

D.P.L. wrote the manuscript, performed the mouse dissections, designed the study, analyzed and arranged the data with input from J.U.R. who prepared the samples, carried out LSFM scans, and analyzed the data. M.S. performed the fluorescence planar microscopy and arranged this data. C.S. revised the final version of the manuscript. F.A. discussed the results, supported the arrangement of data, and revised the manuscript. J.M.G. analyzed the histological data, supervised the work, and designed the outline and supported the writing of the manuscript.

ACKNOWLEDGMENT

The authors thank Sabine Wolfgramm, Bettina Jeep, and Julia Fascher for excellent technical assistance in animal dissection, clearing and embedding procedures, and for performing histology of tissue sections. The project was in part supported by the Bundesministerium fuer Bildung und Forschung, Deutschland, Federal Ministry for Education and Research, Germany ELICIT: 13N14349/50 to J.M.G., University Medical Center Goettingen, Germany and 13N14349/49 to F.A., Max-Planck-Institute for Multidisciplinary Sciences, Goettingen, Germany. Further, the project was in part supported by the Deutsche Forschungsgemeinschaft (DFG, German Research Foundation) under Germany's Excellence Strategy - EXC 2067/1- 390729940 to C.S.

CONFLICT OF INTEREST

The authors declare no competing or financial interests.

ORCID

Jeannine Missbach-Guentner https://orcid.org/0000-0003-1033-8403

REFERENCES

1. Jorgensen A, Svingen T, Miles H, Chetty T, Stukenborg JB, Mitchell RT. Environmental impacts on male reproductive development: lessons from experimental models. *Horm Res Paediatr*. 2021;303-319. https://doi.org/10.1159/000519964
2. Lymperi S, Giwercman A. Endocrine disruptors and testicular function. *Metabolism*. 2018;86:79-90. https://doi.org/10.1016/j.metabol.2018.03.022
3. Rebik K, Wagner JM, Middleton W. Scrotal ultrasound. *Radiol Clin North Am*. 2019;57(3):635-648. https://doi.org/10.1016/j.rcl.2019.01.007
4. Parenti GC, Feletti F, Carnevale A, Uccelli L, Giganti M. Imaging of the scrotum: beyond sonography. *Insights Imaging*. 2018;9(2):137-148. https://doi.org/10.1007/s13244-017-0592-z
5. Tsili AC, Argyropoulou MI, Dolciami M, Ercolani G, Catalano C, Manganaro L. When to ask for an MRI of the scrotum. *Andrology*. 2021;9(5):1395-1409. https://doi.org/10.1111/andr.13032
6. Cerilli LA, Kuang W, Rogers D. A practical approach to testicular biopsy interpretation for male infertility. *Arch Pathol Lab Med*. 2010;134(8):1197-1204. https://doi.org/10.5858/2009-0379-RA.1
7. Sullivan R, Légaré C, Lamontagne-Proulx J, Breton S, Soulet D. Revisiting structure/functions of the human epididymis. *Andrology*. 2019;7(5):748-757. https://doi.org/10.1111/andr.12633
8. Nakata H, Iseki S. Three-dimensional structure of efferent and epididymal ducts in mice. *J Anat*. 2019;235(2):271-280. https://doi.org/10.1111/joa.13006
9. Frohn J, Pinkert-Leetsch D, Missbach-Güntner J, et al. 3D virtual histology of human pancreatic tissue by multiscale phase-contrast X-ray tomography. *J Synchrotron Radiat*. 2020;27(Pt 6):1707-1719. https://doi.org/10.1107/S1600577520011327
10. Pacilè S, Dullin C, Baran P, et al. Free propagation phase-contrast breast CT provides higher image quality than cone-beam breast-CT at low radiation doses: a feasibility study on human mastectomies. *Sci Rep*. 2019;9(1):13762. https://doi.org/10.1038/s41598-019-50075-6
11. Missbach-Guentner J, Pinkert-Leetsch D, Dullin C, et al. 3D virtual histology of murine kidneys -high resolution visualization of pathological alterations by micro computed tomography. *Sci Rep*. 2018;8(1):1407. https://doi.org/10.1038/s41598-018-19773-5
12. Dullin C, Ufartes R, Larsson E, et al. μCT of ex-vivo stained mouse hearts and embryos enables a precise match between 3D virtual histology, classical histology and immunochemistry. *PloS One*. 2017;12(2):e0170597. https://doi.org/10.1371/journal.pone.0170597
13. Tainaka K, Kubota SI, Suyama TQ, et al. Whole-body imaging with single-cell resolution by tissue decolorization. *Cell*. 2014;159(4):911-924. https://doi.org/10.1016/j.cell.2014.10.034
14. Abadie S, Jardet C, Colombelli J, et al. 3D imaging of cleared human skin biopsies using light-sheet microscopy: a new way to visualize in-depth skin structure. *Skin Res Technol*. 2018;24(2):294-303. https://doi.org/10.1111/srt.12429
15. Spalteholz W. Über das Durchsichtigmachen von menschlichen und tierischen Präparaten: nebst Anhang: Über Knochenfärbung. Accessed February 25, 2022. https://digital.zbmed.de/physische_anthropologie/content/titleinfo/555354
16. Yang L, Feuchtinger A, Möller W, et al. Three-dimensional quantitative co-mapping of pulmonary morphology and nanoparticle distribution with cellular resolution in nondissected murine lungs. *ACS Nano*. 2019;13(2):1029-1041. https://doi.org/10.1021/acsnano.8b07524
17. Hahn M, Nord C, Franklin O, et al. Mesoscopic 3D imaging of pancreatic cancer and Langerhans islets based on tissue autofluorescence. *Sci Rep*. 2020;10:18246. https://doi.org/10.1038/s41598-020-74616-6
18. Feuchtinger A, Walch A, Dobosz M. Deep tissue imaging: a review from a preclinical cancer research perspective. *Histochem Cell Biol*. 2016;146(6):781-806. https://doi.org/10.1007/s00418-016-1495-7
19. Kapuscinski J. DAPI: a DNA-specific fluorescent probe. *Biotech Histochem Off Publ Biol Stain Comm*. 1995;70(5):220-233. https://doi.org/10.3109/10520299509108199
20. Paniagua R, Amat P, Nistal M, Martin A. Ultrastructure of Leydig cells in human ageing testes. *J Anat*. 1986;146:173-183.
21. Paniagua R, Nistal M, Amat P, Rodriguez MC, Martin A. Seminiferous tubule involution in elderly men. *Biol Reprod*. 1987;36(4):939-947. https://doi.org/10.1095/biolreprod36.4.939
22. Abd-El-Hafez MA, El-Shafee MD, Omar SH, Aburahma AA, Kamar SS. The ameliorative effect of curcumin on cryptorchid and non-cryptorchid testes in induced unilateral cryptorchidism in albino rat: histological evaluation. *Folia Morphol*. 2021;80(3):596-604. https://doi.org/10.5603/FM.a2020.0084
23. Jamshidian H, Amini E, Karvar M, et al. Effects of opium dependency on testicular tissue in a rat model: an experimental study. *Urol J*. 2019;16(4):375-379. https://doi.org/10.22037/uj.v0i0.4066
24. Yang Y, Honaramooz A. Characterization and quenching of autofluorescence in piglet testis tissue and cells. *Anat Res Int*. 2012;2012:820120. https://doi.org/10.1155/2012/820120
25. Hess RA, Fernandes SAF, Gomes GRO, Oliveira CA, Lazari MFM, Porto CS. Estrogen and its receptors in efferent ductules and epididymis. *J Androl*. 2011;32(6):600-613. https://doi.org/10.2164/jandrol.110.012872
26. Légaré C, Sullivan R. Differential gene expression profiles of human efferent ducts and proximal epididymis. *Andrology*. 2020;8(3):625-636. https://doi.org/10.1111/andr.12745
27. Nakano T, Nakata H, Kadomoto S, et al. Three-dimensional morphological analysis of spermatogenesis in aged mouse testes. *Sci Rep*. 2021;11(1):23007. https://doi.org/10.1038/s41598-021-02443-4
28. Nakata H, Wakayama T, Sonomura T, Honma S, Hatta T, Iseki S. Three-dimensional structure of seminiferous tubules in the adult mouse. *J Anat*. 2015;227(5):686-694. https://doi.org/10.1111/joa.12375
29. Omotehara T, Nakata H, Itoh M. Three-dimensional analysis of mesonephric tubules remodeling into efferent tubules in the male mouse embryo. *Dev Dyn Off Publ Am Assoc Anat*. 2022;251(3):513-524. https://doi.org/10.1002/dvdy.410
30. Nakata H, Omotehara T, Itoh M, Iseki S, Mizokami A. Three-dimensional structure of testis cords in mice and rats. *Andrology*. 2021;9(6):1911-1922. https://doi.org/10.1111/andr.13069
31. McAninch D, Mäkelä JA, La HM, et al. SOX3 promotes generation of committed spermatogonia in postnatal mouse testes. *Sci Rep*. 2020;10(1):6751. https://doi.org/10.1038/s41598-020-63290-3
32. Ferder IC, Fung L, Ohguchi Y, et al. Meiotic gatekeeper STRA8 suppresses autophagy by repressing Nr1d1 expression during spermatogenesis in mice. *PLoS Genet*. 2019;15(5):e1008084. https://doi.org/10.1371/journal.pgen.1008084
33. Moody S, Goh H, Bielanowicz A, Rippon P, Loveland KL, Itman C. Prepubertal mouse testis growth and maturation and androgen production are acutely sensitive to di-n-butyl phthalate. *Endocrinology*. 2013;154(9):3460-3475. https://doi.org/10.1210/en.2012-2227
34. Ruffoli R, Carpi A, Giambelluca MA, Grasso L, Scavuzzo MC, Giannessi F F. Diazepam administration prevents testosterone decrease and lipofuscin accumulation in testis of mouse exposed to chronic noise stress. *Andrologia*. 2006;38(5):159-165. https://doi.org/10.1111/j.1439-0272.2006.00732.x
35. Naeemi S, Eidi A, Khanbabaee R, Sadri-Ardekani H, Kajbafzadeh AM. Differentiation and proliferation of spermatogonial stem cells using a three-dimensional decellularized testicular scaffold: a new method to study the testicular microenvironment in vitro. *Int Urol Nephrol*. 2021;53(8):1543-1550. https://doi.org/10.1007/s11255-021-02877-9
36. Olesen IA, Andersson AM, Aksglaede L, et al. Clinical, genetic, biochemical, and testicular biopsy findings among 1,213 men evaluated for infertility. *Fertil Steril*. 2017;107(1):74-82.e7. https://doi.org/10.1016/j.fertnstert.2016.09.015

37. Hussein SM, El-Fadaly AB, Metawea AG, Khaled BEA. Aging changes of the testis in albino rat: light, electron microscopic, morphometric, immunohistochemical and biochemical study. *Folia Morphol*. 2020;79(3):503-515. https://doi.org/10.5603/FM.a2019.0102
38. Ellenburg JL, Kolettis P, Drwiega JC, et al. Formalin versus bouin solution for testis biopsies: which is the better fixative? *Clin Pathol Thousand Oaks Ventura Cty Calif*. 2020;13:2632010X19897262. https://doi.org/10.1177/2632010X19897262

How to cite this article: Pinkert-Leetsch D, Rost JU, Schmiedeknecht MUH, Stadelmann C, Alves F, Missbach-Guentner J. The murine male reproductive organ at a glance: Three-dimensional insights and virtual histology using label-free light sheet microcopy. *Andrology*. 2022;10:1660–1672. https://doi.org/10.1111/andr.13292